iScience

CellPress
OPEN ACCESS

Article

Replicative stress in gastroesophageal cancer is associated with chromosomal instability and sensitivity to DNA damage response inhibitors

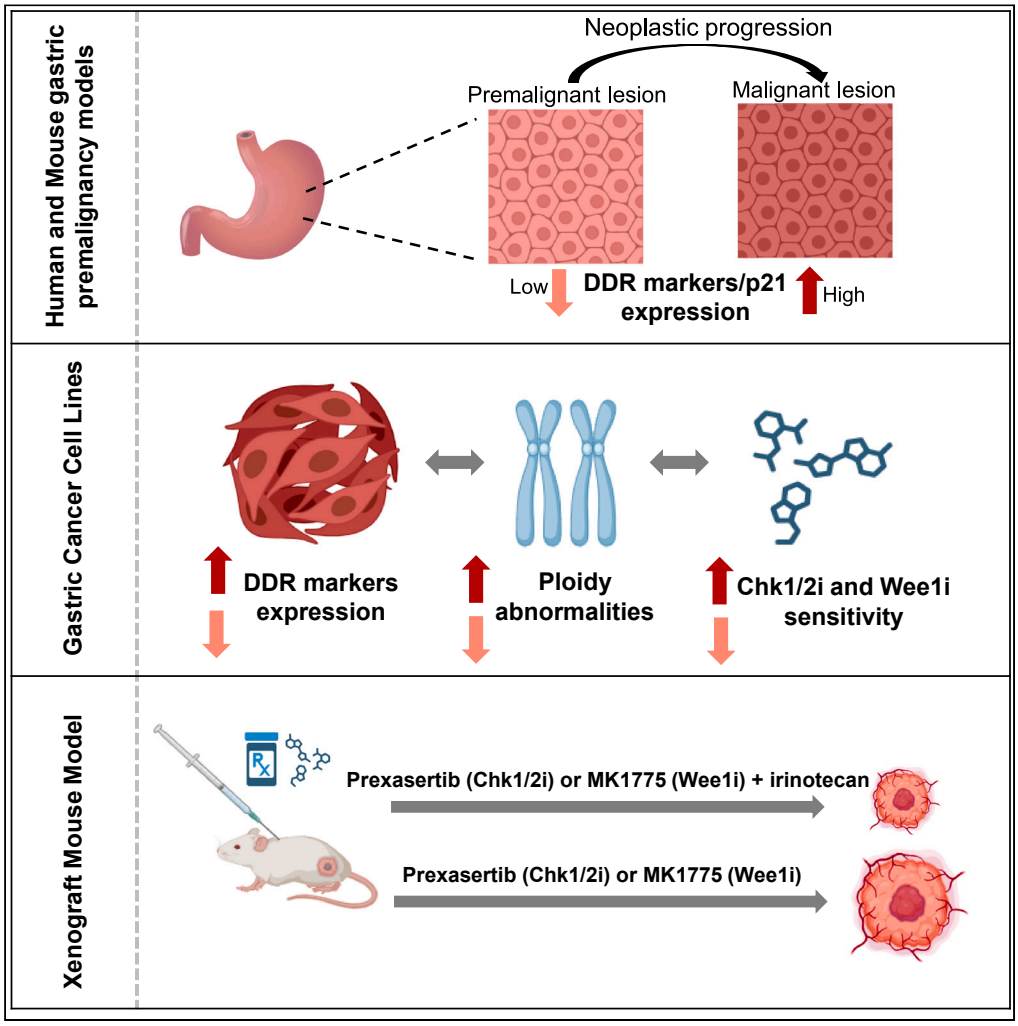

Pranshu Sahgal, Deepa T. Patil, Pratyusha Bala, ..., Zoltan Szallasi, James M. Cleary, Nilay S. Sethi

pranshu_Sahgal@dfci.harvard.edu (P.S.)
nilay_sethi@dfci.harvard.edu (N.S.S.)

Highlights

DDR and replication stress are activated in human and mouse gastric preneoplasia

DDR markers expression correlates with higher ploidy abnormalities in gastric cancer

A cumulative score of ploidy abnormalities (CSPA) predicts DDR inhibitor response

DDR inhibitor irinotecan combo improves anti-tumor effect in gastric cancer models

Sahgal et al., iScience 26, 108169
November 17, 2023
https://doi.org/10.1016/j.isci.2023.108169

iScience

CellPress
OPEN ACCESS

Article

Replicative stress in gastroesophageal cancer is associated with chromosomal instability and sensitivity to DNA damage response inhibitors

Pranshu Sahgal,[1,2,3,8,*] Deepa T. Patil,[4,12] Pratyusha Bala,[1,2,3,12] Zsofia M. Sztupinszki,[5,8] Viktoria Tisza,[1,10] Sandor Spisak,[1,10] Anna G. Luong,[1] Brandon Huffman,[1] Aurel Prosz,[5] Harshabad Singh,[1,2,9] Jean-Bernard Lazaro,[6,7] Zoltan Szallasi,[5,8,11] James M. Cleary,[1,9] and Nilay S. Sethi[1,2,3,9,13,*]

SUMMARY

Gastroesophageal adenocarcinoma (GEA) is an aggressive malignancy with chromosomal instability (CIN). To understand adaptive responses enabling DNA damage response (DDR) and CIN, we analyzed matched normal, premalignant, and malignant gastric lesions from human specimens and a carcinogen-induced mouse model, observing activation of replication stress, DDR, and p21 in neoplastic progression. In GEA cell lines, expression of DDR markers correlated with ploidy abnormalities, such as number of high-level focal amplifications and whole-genome duplication (WGD). Integrating *TP53* status, ploidy abnormalities, and DDR markers into a compositive score helped predict GEA cell lines with enhanced sensitivity to Chk1/2 and Wee1 inhibition, either alone or combined with irinotecan (SN38). We demonstrate that Chk1/2 or Wee1 inhibition combined with SN38/irinotecan shows greater anti-tumor activity in human gastric cancer organoids and an *in vivo* xenograft mouse model. These findings indicate that specific DDR biomarkers and ploidy abnormalities may predict premalignant progression and response to DDR pathway inhibitors.

INTRODUCTION

Gastroesophageal adenocarcinoma (GEA) is a leading cause of death globally and improvement in patient outcomes has been hampered by multiple issues, including failure to identify patients with high-risk precancerous lesions and limited targeted therapy options for patients with advanced disease. The Cancer Genome Atlas (TCGA) project's recent molecular classification has characterized GEA into 4 subtypes: microsatellite-unstable, Epstein-Barr virus-positive, chromosomal-instability (CIN), and genomically stable (GS) cancers. These classifications have given insight into the molecular features of these subtypes and help advance the field of early diagnosis and targeted therapies in GEA.[1]

The most common subtype is CIN, seen in 50% of GEA patients. The molecular features associated with CIN and subsequent consequences of CIN are still poorly understood.[2,3] Nevertheless, CIN is positively correlated with multidrug resistance and ploidy abnormalities, including whole-genome duplication (WGD) and high-level focal amplification events. In addition, recent studies have hypothesized that replicative stress, defined as the presence of stalled replication forks leading to single-strand DNA and possible fork collapse, plays a major role in CIN development. Several proteins in the DNA damage response (DDR) pathway, including Chk1 and Wee1, compensate for replicative stress by slowing the cell cycle and promoting the stability of stalled replication forks.[4,5] When these compensatory mechanisms fail, replication forks can collapse and lead to the generation of double-strand DNA breaks, promoting CIN.

We hypothesized that high levels of replicative stress are present during the evolution of CIN in GEA. We evaluated the expression of DDR markers in human and mouse specimens with matched normal, premalignant, and malignant lesions. Further, we assessed whether GEA cell lines with different levels of DDR and associated ploidy abnormalities correlate with sensitivity to DDR inhibitors in GEA. Recent preclinical

[1]Department of Medical Oncology, Dana-Farber Cancer Institute, Boston, MA 02215, USA
[2]Department of Medicine, Brigham and Women's Hospital and Harvard Medical School, Boston, MA 02115, USA
[3]Broad Institute of Massachusetts Institute of Technology (MIT) and Harvard University, Cambridge, MA 02142, USA
[4]Department of Pathology, Brigham and Women's Hospital, Harvard Medical School, Boston, MA 02215, USA
[5]Danish Cancer Institute, 2100 Copenhagen, Denmark
[6]Department of Radiation Oncology, Dana-Farber Cancer Institute, Boston, MA 02215, USA
[7]Center for DNA Damage and Repair (CDDR), Dana-Farber Cancer Institute, Boston, MA 02215, USA
[8]Computational Health Informatics Program, Boston Children's Hospital, Boston, MA 02115, USA
[9]Division of Gastrointestinal Oncology, Department of Medical Oncology, Dana-Farber Cancer Institute, Boston, MA 02215, USA
[10]Institute of Enzymology, Research Centre for Natural Sciences, Eötvös Loránd Research Network, 1117 Budapest, Hungary
[11]Department of Bioinformatics and Department of Pathology, Forensic and Insurance Medicine, Semmelweis University, 1091 Budapest, Hungary
[12]These authors contributed equally
[13]Lead contact
*Correspondence: pranshu_Sahgal@dfci.harvard.edu (P.S.), nilay_sethi@dfci.harvard.edu (N.S.S.)
https://doi.org/10.1016/j.isci.2023.108169

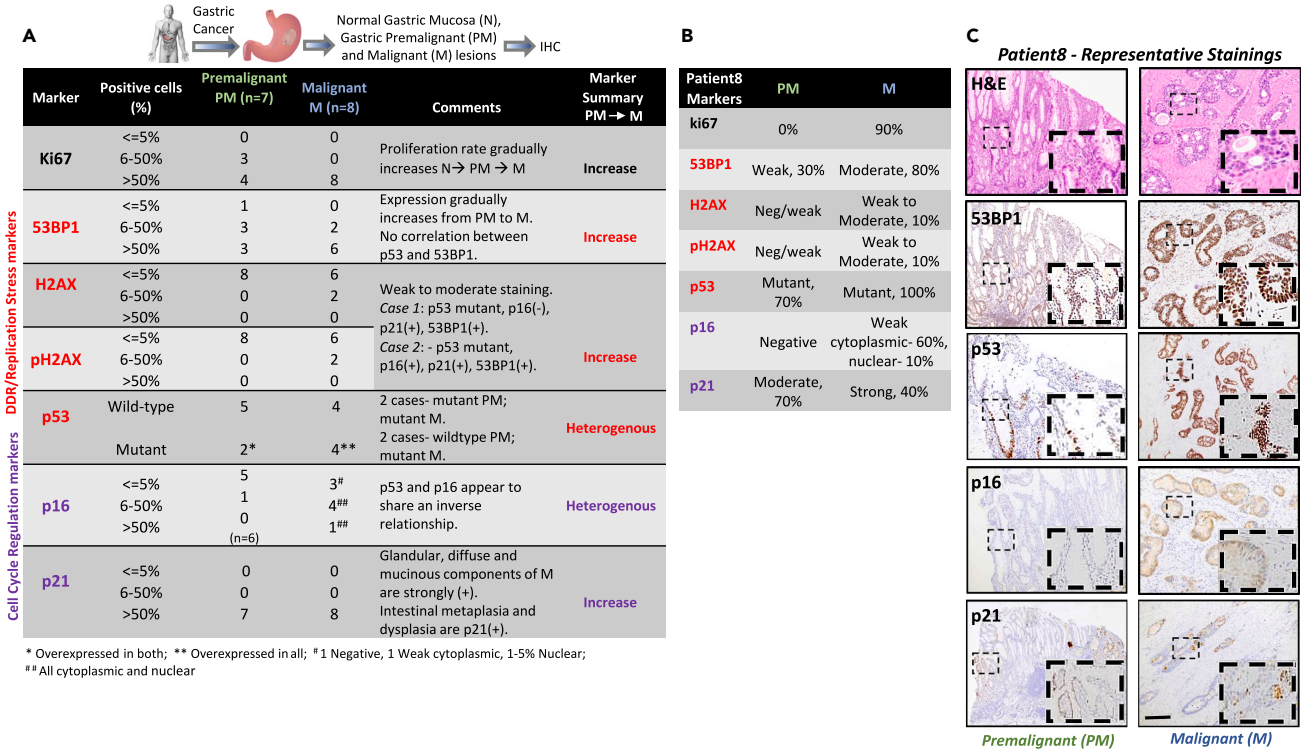

Marker	Positive cells (%)	Premalignant PM (n=7)	Malignant M (n=8)	Comments	Marker Summary PM → M
Ki67	<=5%	0	0	Proliferation rate gradually increases N→ PM → M	Increase
	6-50%	3	0		
	>50%	4	8		
53BP1	<=5%	1	0	Expression gradually increases from PM to M. No correlation between p53 and 53BP1.	Increase
	6-50%	3	2		
	>50%	3	6		
H2AX	<=5%	8	6	Weak to moderate staining. *Case 1*: p53 mutant, p16(-), p21(+), 53BP1(+). *Case 2*: - p53 mutant, p16(+), p21(+), 53BP1(+).	Increase
	6-50%	0	2		
	>50%	0	0		
pH2AX	<=5%	8	6		
	6-50%	0	2		
	>50%	0	0		
p53	Wild-type	5	4	2 cases- mutant PM; mutant M. 2 cases- wildtype PM; mutant M.	Heterogenous
	Mutant	2*	4**		
p16	<=5%	5	3#	p53 and p16 appear to share an inverse relationship.	Heterogenous
	6-50%	1	4##		
	>50%	0 (n=6)	1##		
p21	<=5%	0	0	Glandular, diffuse and mucinous components of M are strongly (+). Intestinal metaplasia and dysplasia are p21(+).	Increase
	6-50%	0	0		
	>50%	7	8		

* Overexpressed in both; ** Overexpressed in all; # 1 Negative, 1 Weak cytoplasmic, 1-5% Nuclear; ## All cytoplasmic and nuclear

Patient8 Markers	PM	M
ki67	0%	90%
53BP1	Weak, 30%	Moderate, 80%
H2AX	Neg/weak	Weak to Moderate, 10%
pH2AX	Neg/weak	Weak to Moderate, 10%
p53	Mutant, 70%	Mutant, 100%
p16	Negative	Weak cytoplasmic- 60%, nuclear- 10%
p21	Moderate, 70%	Strong, 40%

Figure 1. Evaluation of DDR and cell cycle markers in matched normal, premalignant, and malignant human gastric specimens

(A) Tabulated summary of IHC stainings indicating the number of premalignant (green) and malignant (blue) gastric lesions scored for each staining criterion. DDR/replication stress markers- 53BP1, H2AX, pH2AX, p53 in red; Cell cycle regulators- p16, p21 in purple.

(B) Summary of the stainings (DDR markers and the cell cycle regulation markers) in paired premalignant and malignant gastric lesions from gastric cancer patient8. PM = Premalignant gastric lesion, M = Malignant gastric lesion.

(C) Representative IHC images of paired premalignant and malignant gastric lesions from a gastric cancer patient (patient8) stained for DDR markers and cell cycle regulation markers, including H&E staining. Insets represent the zoomed area for each image. Scale bar: 100 μM.

and clinical studies suggest that the chemotherapeutic agents that generate replication stress are more effective in different cancers when combined with Chk1 inhibitors.[6] Therefore, we also examined anti-tumor properties of DDR inhibitors in combination with two commonly used chemotherapeutic agents, showing greater therapeutic potential for one pair.

RESULTS

Activation of select DDR markers in human gastric premalignancy progression

The progression from premalignancy to cancer is associated with replication stress that leads to DNA double-strand breaks (DSBs) and genomic instability.[7] To define the role of DDR/replication stress in the evolution of GEA, we procured human gastric specimens from 8 patients that had matched normal, premalignant, and malignant lesions (Table S1). Using immunohistochemistry (IHC), we evaluated the levels of phospho-H2AX (pH2AX) and 53BP1, 2 well-known markers of DNA DSBs and replicative stress.[8–10] We observed that 53BP1 levels increased during neoplastic progression, with invasive adenocarcinoma displaying the highest levels of 53BP1 for nearly all patients (Figures 1A–1C; Table S2). While levels of pH2AX were largely absent in normal and premalignant lesions, moderate staining was observed in malignant lesions of 2 patients (Figures 1A, 1B, and S1A; Table S2). These observations suggest that human gastric premalignant to malignant progression is associated with DNA DSBs and replication stress.

Unlike colorectal cancer, GEA harbor early *TP53* mutations, often preceding dysplasia.[11–15] As GEA evolves, CIN ensues, selecting for amplification of oncogenes and deep deletions of tumor suppressor genes.[16,17] We recently showed that *TP53*(p53)/*CDKN2A*(p16) co-altered premalignant gastric organoids derived from a mouse model displayed evidence of early CIN, which was associated with the activation of replication stress and DDR pathways.[11] Based on this understanding, we next examined the status of cell cycle regulation markers (p16 and p21) and p53, which functions both as a replication stress marker and cell cycle regulator. We observed marked heterogeneity in p53 and p16 levels among premalignant and malignant lesions, even within a patient. Lesions from the same patient expressed both wild-type (WT) and mutant p53 as well as areas of p16 positivity and negativity (Figure 1A). Interestingly, mutant p53 and p16 expression appeared to share an inverse relationship, especially in malignant lesions; p53 WT cells displayed p16 expression whereas p53 mutant cells were p16 negative (Figures 1A–1C and S1B; Table S3). A downstream effector of p53, p21 induces cell-cycle arrest.[18] Notably, we observed

A

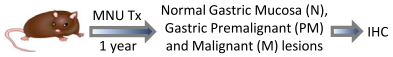

Marker	Tissue	Mouse1	Mouse2	Mouse3	Mouse4	Marker Summary N → PM → M
(H&E) Dysplasia score		3-4 (LGD-HGD)	3-4 (LGD-HGD)	3 (LGD)	5*	
ki67	N	0%	Foveolar-0%	Foveolar-0%	Foveolar-0%	Increase
	PM	40%	40%	80%	50%	
	M				50%	
pH2AX	N	Negative	Negative	Negative	Negative	Increase
	PM	Negative	Negative	Weak, heterogenous 20%	Weak, heterogenous 5%	
	M				Weak, heterogenous 5%	
p53	N	WT (10%)		WT (10%)	WT (10%)	Increase
	PM	WT (30%)	WT (30%)	Weak to moderate, 90%	Weak to Moderate, 30%	
	M				30% weak	
p21	N	Foveolar-0%	Foveolar-0%	Foveolar-0%	Foveolar-0%	Increase/ Heterogenous
	PM	Heterogenous 20-30%	Heterogenous 20-30%	Heterogenous 60%	Heterogenous 30-40%	
	M				Heterogenous 60-70%	

LGD=low grade dysplasia
HGD=high grade dysplasia

*Intramucosal adenocarcinoma with low-grade and high-grade background
WT=wildtype

B

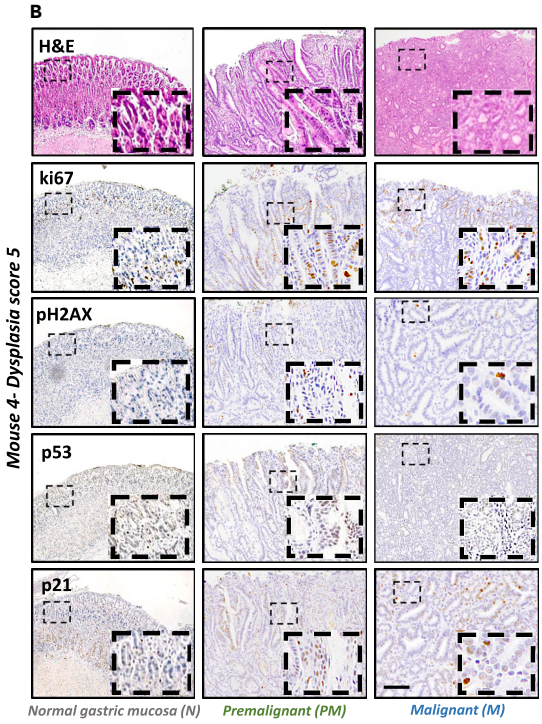

Figure 2. Evaluation of DDR markers linked with dsDNA breaks and cell cycle regulation markers in the carcinogen-induced mouse model of gastric premalignancy

(A) Summary of dysplasia grade and staining pattern of proliferation marker ki67, DDR marker pH2AX, and cell cycle regulation markers (p53 and p21) in paired normal (gray), premalignant (green), and malignant (blue) gastric lesions of four MNU treated mice.

(B) Representative IHC images of staining pattern of proliferation marker ki67, DDR marker pH2AX, and cell cycle regulation markers (p53 and p21) in paired normal, premalignant, and malignant gastric lesions of MNU treated mouse4 (dysplasia score 5). Scale bar: 100 μM.

a gradual increase in p21 levels in GEA progression; malignant lesions demonstrated significantly higher expression of p21 compared to normal and premalignant lesions in almost all patients. The glandular, diffuse, and mucinous components of adenocarcinoma showed strong p21 staining, while intestinal metaplasia and dysplasia showed moderate p21 staining (Figures 1A–C and S1B; Table S3). p21 staining appeared to be independent of mutant p53 expression in gastric cancer progression (Figures 1B, 1C, and S2B). Despite the heterogeneity in expression of cell cycle regulators, proliferation as measured by ki67 levels gradually increased from normal to malignant lesions (Table S1). These results indicate that p53 and p16 expression is heterogenous within lesions and through cancer progression, whereas p21 gradually increases from normal to malignant lesions independent of p53 status.

Evaluation of DDR markers in carcinogen-induced mouse model of gastric premalignancy

We next evaluated our panel of biomarkers in a carcinogen-induced (MNU) mouse model of gastric premalignancy and cancer to validate our human observations. Mice exposed to drinking water containing MNU developed premalignant and malignant gastric lesions after 1 to 1.5 years.[11] We examined 4 mice treated with MNU that developed varying degrees of dysplasia and cancer (Figures 2A and 2B), staining formalin-fixed tissue for markers of dsDNA breaks, DDR pathway, and cell cycle regulators. Technical immunostaining limitations precluded interpretation of slides stained for H2AX (dsDNA breaks), 53BP1 (DDR pathway), and p16 (cell cycle). As expected, premalignant and malignant lesions demonstrated greater proliferation compared to normal gastric tissue by Ki67 IHC. We also found the levels of pH2AX, p53, and p16 expression were similar in our mouse lesions compared to the human specimen (Figures 2A, 2B, and S2A); pH2AX was expressed in a premalignant gastric lesion from one mouse (mouse #3) and malignant lesion from another one (mouse #4), but not in normal gastric tissue from any mice. While p53 expression was low in normal gastric tissue, premalignant lesions in mouse #3 and #4 displayed higher p53 expression, consistent with it being mutated. Similarly, p21 was not expressed in normal gastric tissue but was expressed to varying degrees in premalignant and malignant lesions in all 4 mice, with the strongest heterogeneous staining in mouse #3 and #4 (Figures 2A, 2B, and S2A). These results indicate that, like human gastric premalignancy progression, a carcinogen-induced mouse model of gastric adenocarcinoma progression displays increased levels of DDR marker pH2AX and cell cycle regulator p21, with p21 expression independent of p53 mutation status.

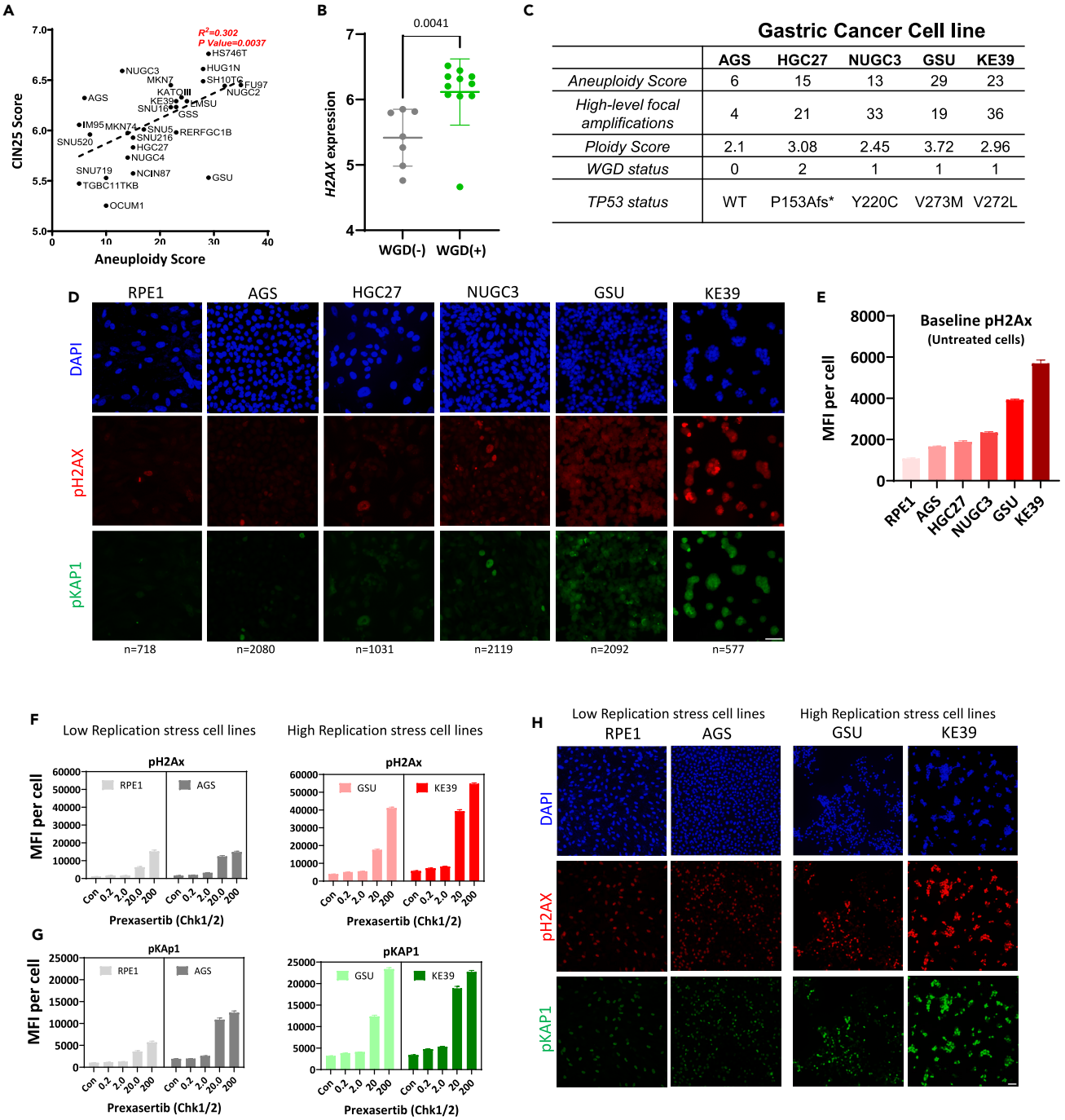

Figure 3. Aneuploidy correlates and H2AX expression correlates with DDR pathway activity in gastric cancer

(A) Correlation plot between aneuploidy score and CIN25 score (DNA damage checkpoint expression) for the CCLE gastric cancer cell lines. R squared value and p value calculated by simple linear correlation analysis.

(B) H2AX expression (log2(TPM+1)) between "No WGD (0)" (gray) and "with WGD (1/2)" (green) groups of gastric cancer cell lines available in the BROAD institute PRISM repurposing drug screen dataset; difference between the H2AX expression is represented as the mean ± S.D.; p value calculated by unpaired t test.

(C) Ploidy abnormalities scores and p53 status for the five gastric cancer cell lines.

(D) Representative immunofluorescence images of pH2AX (red) and pKAP1 (green) stainings in untreated five gastric cancer cell lines and RPE1 cells (non-neoplastic cell line) representing intrinsic replication stress/double-stranded DNA breaks (DSBs); nucleus stained with DAPI (blue); Scale bar: 50 μm.

(E) Quantification of pH2AX and pKAP1 in indicated cell lines expressed as mean fluorescence intensity per cell (MFI) ± S.D from the following number of cells-RPE1-718, AGS- 2080, HGC27, 1031, NUGC3- 2119, GSU- 2092, KE39- 577.

Figure 3. *Continued*

(F) Quantification of pH2AX staining in prexasertib (Chk1/2) dose-dependent induced replication stress in cell lines with "intrinsic low-replication stress"-RPE1, AGS (gray) and "intrinsic high-replication stress"- GSU, KE39 (red). Data expressed as mean fluorescence intensity (MFI) of pH2AX signal per cell ± S.D from the following number of cells- RPE1: Control-718, 0.2nM-888, 2.0nM-524, 20.0nM-570, 200.0nM- 350; AGS: Control-2080, 0.2nM-1487, 2.0nM-1996, 20.0nM-1211, 200.0nM- 1396; GSU: Control-2092, 0.2nM-3319, 2.0nM-4035, 20.0nM-2057, 200.0nM-2402; KE39: Control-577, 0.2nM-1004, 2.0nM-1022, 20.0nM-728, 200.0nM-958.

(G) Quantification of pKAP1 staining in prexasertib (Chk1/2) dose-dependent induced replication stress in cell lines with "intrinsic low-replication stress"-RPE1, AGS (gray) and "intrinsic high-replication stress"- GSU, KE39 (green). Data expressed as mean fluorescence intensity of pKAP1 signal per cell ±S.D from the following number of cells- RPE1: Control-718, 0.2nM-888, 2.0nM-524, 20.0nM-570, 200.0nM- 350; AGS: Control-2080, 0.2nM-1487, 2.0nM-1996, 20.0nM-1211, 200.0nM- 1396; GSU: Control-2092, 0.2nM-3319, 2.0nM-4035, 20.0nM-2057, 200.0nM-2402; KE39: Control-577, 0.2nM-1004, 2.0nM-1022, 20.0nM-728, 200.0nM-958.

(H) Representative immunofluorescence images of pH2AX (red) and pKAP1 (green) stainings in prexasertib (20nM) treated cell lines with intrinsic "low-replication stress"-RPE1, AGS, and intrinsic "high-replication stress"- GSU, KE39; Scale bar: 50μm.

Evaluation of DDR markers in TCGA cohort of stomach adenocarcinoma

To further characterize components of the DDR pathway in human gastric cancer, we evaluated *H2AX* and *TP53BP1* expression in the TCGA stomach adenocarcinoma (STAD) dataset.[19] We observed higher expression of both *H2AX* and *TP53BP1* in gastric adenocarcinoma samples compared with normal gastric tissue (Figures S2B). Interestingly, *H2AX* but not *TP53BP1* expression was significantly higher in *TP53* mutant gastric adenocarcinomas compared to *TP53* WT tumors (Figure S2C). Next, we evaluated the expression of *H2AX* and *TP53BP1* in Lauren's classification subtypes of gastric adenocarcinoma. Lauren's criteria is based on distinct clinical and molecular characteristics that divide gastric adenocarcinoma into intestinal and diffuse subtypes and is the most widely used histological classification for gastric adenocarcinoma.[20] We observed a significantly higher expression of *H2AX* and not *TP53BP1* in the intestinal subtype than in the diffuse subtype (Figure S2D). Furthermore, *TP53* mutations were more enriched in intestinal subtype patients and in CIN tumors (Figure S2E). These observations suggest the patients with gastric adenocarcinoma that harbor p53 mutations and/or intestinal subtype histology express higher levels of DDR markers such as *H2AX*.

DDR pathway activity is associated with ploidy abnormalities in gastric cancer

Since the majority of GEA exhibit ploidy defects as a result of CIN,[2] we next evaluated the relationship between CIN and elevated markers of DDR or replication stress. To assess CIN in gastric cancer cell lines, we utilized the CIN25 score,[21] a gene expression-based validated signature of CIN that predicts clinical outcomes across different human cancers. Indeed, gastric cancer cell lines in the Cancer Cell Line Encyclopedia (CCLE)[22] displayed a strong correlation between the CIN25 score and a recently reported computational metric of aneuploidy (score based on Cohen-Shahir et al., 2021[23]) (Figure S3A). Importantly, *H2AX* expression correlated with high CIN25 score in gastric cancer cell lines (Figure 3A). In our analysis, we also found a positive correlation between the aneuploidy score and high-level focal amplifications (Figure S3B), a unique characteristic of gastric cancer evolution,[16] a ploidy score (Figure S3C) and whole genome doubling (WGD) (Figure S3D) (both scores based on Ghandi et al., 2019[24]). Interestingly, gastric cancer cell lines with WGD have significantly higher expression of *H2AX* compared to ones without WGD (Figure 3B). These analyses suggest that DDR pathway markers, at least *H2AX*, track with WGD and ploidy defects in gastric cancer.

To validate the *in silico* analyses, we evaluated five gastric cancer cell lines (AGS, HGC27, HUGC3, GSU, and KE39) that showed varying levels of aneuploidy (Figure 3C) and one non-neoplastic diploid cell line (RPE1). We determined levels of pH2AX and pKAP1 in these cell lines to assess intrinsic DNA DSBs/replication stress. In response to DNA damage and replication stress, KAP1 is phosphorylated at serine 473.[25] As expected, RPE1 cells showed minimal staining for pH2AX and pKAP1. Similarly, low levels of pH2AX and pKAP1 were observed in AGS, a TP53 WT gastric cancer cell line displaying the least aneuploidy defects. In contrast, we observed strong and moderate pH2AX and pKAP1 staining in high (KE39 and GSU) and intermediate (HGC27 and NUGC3) aneuploidy cell lines, respectively (Figure 3D). Importantly, since dsDNA breaks correlate with DDR response, these markers tracked with one another. As such, pH2AX and pKAP1 levels positively correlated with the degree of various ploidy defect measurements and p53 mutation status (Figure 3E). GSU and KE39 not only demonstrated greater baseline levels of DNA DSB and replication stress compared to RPE1 and AGS as measured by pH2AX and pKAP1, but also showed a more dramatic, dose-dependent induction when treated with prexasertib,[26] a well-known Chk1/2 inhibitor (Figures 3F–3H). These results demonstrate a correlation between broad measures of ploidy defects and DDR pathway activity in gastric cancer.

Gastric cancer with ploidy abnormalities and high *H2AX* expression are more sensitive to DDR pathway inhibitors

Based on these results, we hypothesized that, in addition to the degree of aneuploidy, the level of DDR pathway response to DNA DSBs and replication stress might correlate with sensitivity to drugs that inhibit DNA-damage checkpoint proteins. In other words, the effectiveness of DDR pathway inhibitors for gastric tumors may depend on levels of DDR activity in the setting of aneuploidy. To test this hypothesis, we used data from the PRISM repurposing drug screen of the BROAD Institute[27] to characterize the sensitivity of the gastric cancer cell lines for DDR pathway inhibitors. Of all the inhibitors examined (Table S4), there was a positive association between higher aneuploidy score and sensitivity to multiple Chk1/2 inhibitors (prexasertib, PF-477736, and Rabusertib) (Figures 4A and S4A). Moreover, higher aneuploidy score and Wee1 inhibitor MK1775 (AZD1775) sensitivity also showed a positive correlation (Figure 4G). Similarly, the CIN25 score in gastric cancer cell lines positively correlated with Chk1/2 inhibitor sensitivity (Figure S4B).

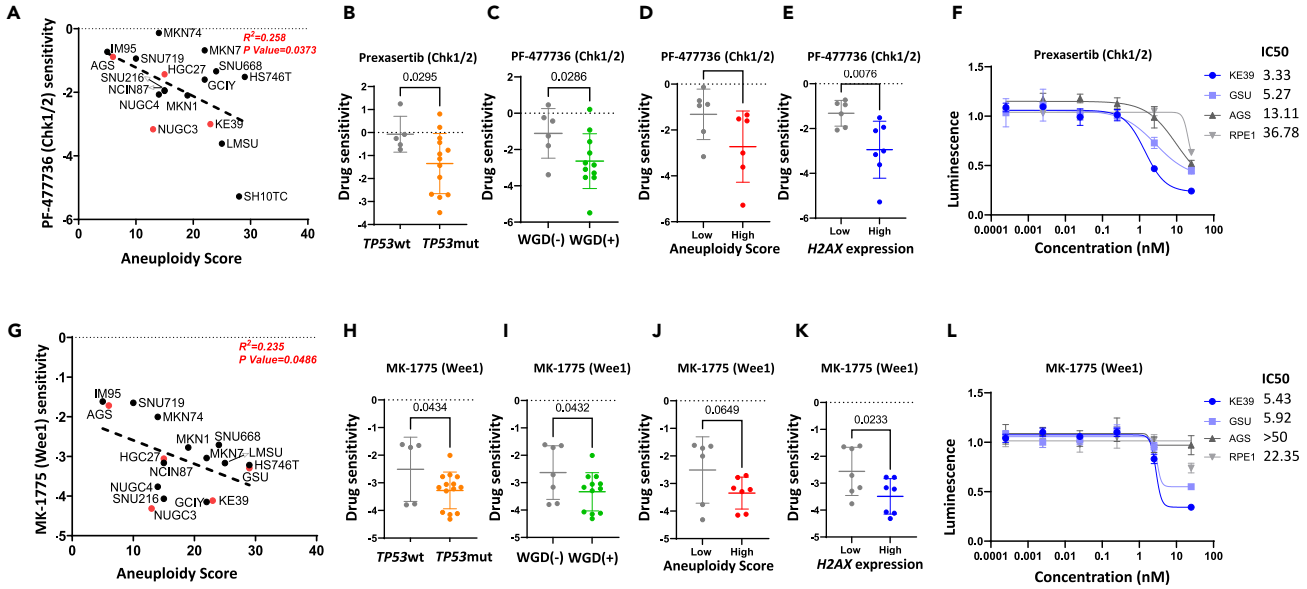

Figure 4. Gastric cancer with ploidy abnormalities and high *H2AX* expression are more sensitive to DDR pathway inhibitors

(A) Correlation plot between aneuploidy score and PF-477736 (Chk1/2) sensitivity (log2 fold change) for the CCLE gastric cancer cell lines; cell lines used in this study marked in red; R squared value and p value calculated by simple linear correlation analysis.

(B) Prexasertib (Chk1/2) sensitivity between "*TP53* wt" and "*TP53* mut" groups of gastric cancer cell lines BROAD institute PRISM repurposing drug screen dataset; difference between the prexasertib (Chk1/2) sensitivity (log2 fold change) is represented as the mean ± S.D.; p value calculated by unpaired t test.

(C) PF-477736 (Chk1/2) sensitivity between "No WGD (0)" (gray) and "with WGD (1/2)" (green) groups of gastric cancer cell lines available in BROAD institute PRISM repurposing drug screen dataset; difference between the PF-477736 (Chk1/2) sensitivity (log2 fold change) is represented as the mean ± S.D.; p value calculated by unpaired t test.

(D) PF-477736 (Chk1/2) sensitivity between low aneuploidy score (gray) and high aneuploidy score (red) groups of gastric cancer cell lines available in BROAD institute PRISM repurposing drug screen dataset; difference between the PF-477736 (Chk1/2) sensitivity (log2 fold change) is represented as the mean ± S.D.; p value calculated by unpaired t test.

(E) PF-477736 (Chk1/2) sensitivity between "low H2AX expressing" (gray) and "high *H2AX* expressing" (green) groups (log2(TPM+1)) of gastric cancer cell lines available in BROAD institute PRISM repurposing drug screen dataset; difference between the PF-477736 (Chk1/2) sensitivity (log2 fold change) is represented as the mean ± S.D.; p value calculated by unpaired t test.

(F) Dose-response curve of non-neoplastic cell line RPE1, low replication-stress (gray)-AGS, and high replication-stress (blue)-KE39, GSU gastric cancer cell lines to indicated concentrations of prexasertib (Chk1/2); best-fit IC50 scores are displayed; data presented as mean ± S.D. of four culture replicates at each indicated dose.

(G) Correlation plot between aneuploidy score and MK-1775 (Wee1) sensitivity (log2 fold change) for the CCLE gastric cancer cell lines; cell lines used in this study marked in red; R squared value and p value calculated by simple linear correlation analysis.

(H) MK-1775 (Wee1) sensitivity between "*TP53* wt" and "*TP53* mut" groups of gastric cancer cell lines BROAD institute PRISM repurposing drug screen dataset; the difference between the MK-1775 (Wee1) sensitivity (log2 fold change) is represented as the mean ± S.D.; p value calculated by unpaired t test.

(I) MK-1775 (Wee1) sensitivity between "No WGD (0)" (gray) and "with WGD (1/2)" (green) groups of gastric cancer cell lines available in BROAD institute PRISM repurposing drug screen dataset; difference between the MK-1775 (Wee1) sensitivity (log2 fold change) is represented as the mean ± S.D.; p value calculated by unpaired t test.

(J) MK-1775 (Wee1) sensitivity between low aneuploidy score (gray) and high aneuploidy score (red) groups of gastric cancer cell lines available in BROAD institute PRISM repurposing drug screen dataset; difference between the MK-1775 (Wee1) sensitivity (log2 fold change) is represented as the mean ± S.D.; p value calculated by unpaired t test.

K) MK-1775 (Wee1) sensitivity between "low *H2AX* expressing" (gray) and "high *H2AX* expressing" (blue) groups (log2(TPM+1)) of gastric cancer cell lines available in BROAD institute PRISM repurposing drug screen dataset; difference between the MK-1775 (Wee1) sensitivity (log2 fold change) is represented as the mean ± S.D.; p value calculated by unpaired t test.

(L) Dose-response curve of non-neoplastic cell line RPE1, low replication-stress (gray)-AGS, and high replication-stress (blue)-KE39, GSU gastric cancer cell lines to indicated concentrations of MK-1775 (Wee1); best-fit IC50 scores are displayed; data presented as mean ± S.D. of four culture replicates at each indicated dose.

Based on these observations and to further build confidence in our results, we divided the gastric cancer cell lines into 2 groups (quartiles) based on *TP53* status and "high or low" ploidy abnormalities (aneuploidy score, WGD, CIN25 score, high amplitude focal amplifications, and ploidy score). Gastric cancer cell lines with *TP53* mutation and a high degree of ploidy abnormalities were significantly more sensitive to the Chk1/2 (Figures 4B–4D) and Wee1 (Figures 4H–4J) inhibitors (Figures S4C–S4G). We also observed that gastric cancer cell lines with specific ploidy defects were sensitive to a subset of ATR inhibitors (AZD6738 for high ploidy cell lines and ETP-46464 for high CIN25 cell lines), but validation experiments using AZD6738 were not able to confirm these results (Figure S4H).

A

Parameters	IM95	NCIN87	GSU	SNU719	SNU668	NUGC4	KE39	AGS	2313287	MKN74	NUGC3	SNU216	HGC27	HS746T	MKN7	LMSU	SH10TC
TP53 status	1	2	2	1	2	1	2	1	1	2	2	2	2	2	2	2	2
Aneuploidy score	1	1	2	1	2	1	2	1	1	1	1	1	1	2	2	2	2
High amplitude focal amplifications	1	1	1	1	2	2	2	1	1	2	2	2	2	2	2	2	2
Ploidy score	1	1	2	1	1	1	2	1	1	1	1	1	2	2	2	2	2
WGD	0	0	1	0	0	0	1	0	0	1	1	1	2	2	2	1	2
CIN25 score	1	1	1	1	1	1	2	2	1	1	2	1	1	2	2	2	2
H2AX Expression	1	1	1	1	1	1	2	1	1	2	2	2	2	2	2	2	2
Cumulative Score of Ploidy Abnormalities (CSPA)	6	7	10	6	9	7	13	7	6	10	11	10	12	14	14	13	14
Prexasertib sensitivity	1.25	0.81	0.23	-0.08	-0.24	-0.26	-0.43	-0.53	-0.74	-0.77	-0.93	-1.14	-1.43	-1.95	-2.68	-2.71	-3.48

R^2=0.623
P= 0.000.

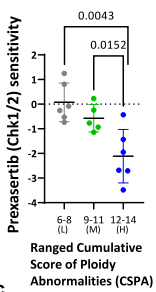

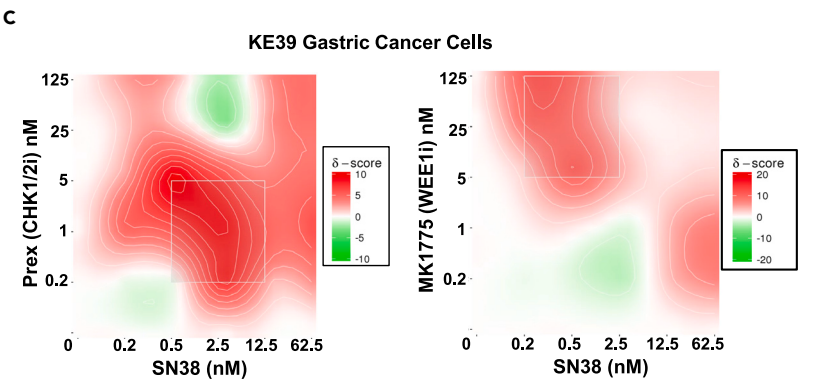

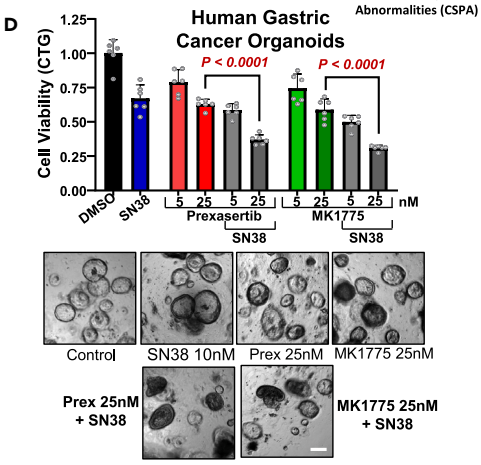

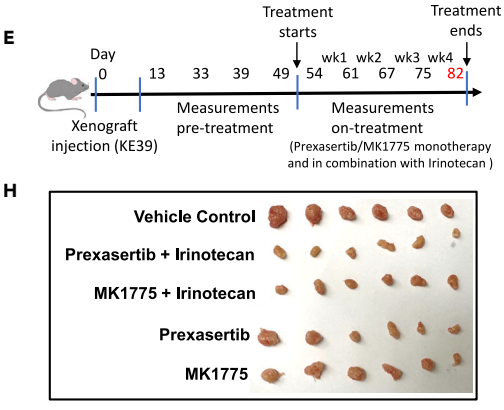

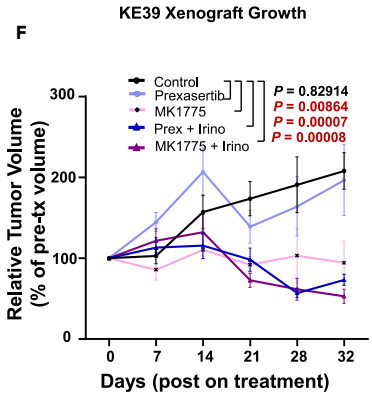

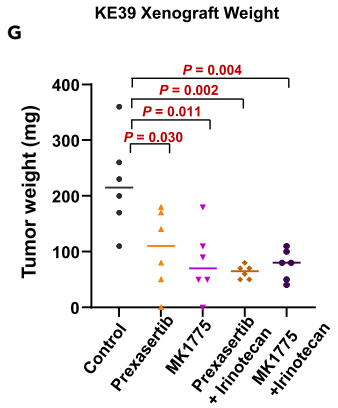

Figure 5. Combination of DDR pathway inhibitors and irinotecan improves anti-tumor activity in gastric cancer models compared to monotherapy

(A) Heatmap table representing the correlation between the Cumulative score of ploidy abnormalities and prexasertib sensitivity for gastric cancer cell lines in CCLE. The scoring scheme is as follows: TP53 status: wt = 1, mut = 2; Aneuploidy score: 15 and less than 15 = 1, more than 15 = 2; High amplitude focal amplifications: 20 and less than 20 = 1, more than 20 = 2; Ploidy score: 2.5 and less than 2.5 = 1, more than 2.5 = 2; WGD: No WGD = 0, WGD 1 = 1, WGD2 = 2; CIN25 score: 6.1 and less than 6.1 = 1, more than 6.1 = 2; H2AX Expression: 6 and less than 6 = 1, more than 6 = 2. R squared value and p value calculated by simple linear correlation analysis.

(B) Prexasertib sensitivity between three sub-ranged "Cumulative score of ploidy abnormalities" groups of gastric cancer cell lines BROAD institute PRISM repurposing drug screen dataset; difference between the prexasertib (Chk1/2) sensitivity (log2 fold change) is represented as the mean ± S.D.; L = low, M = medium, H = high; p value calculated by unpaired t test.

(C) KE39 cells were treated with increasing concentrations of prexasertib (left) or MK1775 (right) in combination with increasing concentrations of SN38. Viability in the treatment groups was normalized to DMSO control. Analysis of inhibition-synergistic effect was performed by SynergyFinder using Zero Interaction Potency (ZIP) model. The inhibition rate was used to calculate ZIP synergy score. The white box indicates area (doses) with most drug synergy.

(D) Cell viability of patient-derived gastric cancer organoids treated with vehicle, SN38, prexasetib, MK1775, prexasetib+SN38 and MK1775+SN38. Dark organoids indicate apoptotic organoids. Data presented as mean ± S.D; p value calculated by unpaired t test. Representative images below. Scale bar: 50 μm.

(E) A schematic showing the timeline of the KE39 xenograft mouse experiment (n = 6 per group).

Figure 5. *Continued*

(F) Change in xenograft volumes in mice treated with indicated control or drug(s) over time. Data are mean ± SEM; p value calculated by two-way ANOVA test.

(G) Measurement of tumor weights at the end of the treatment in indicated control and treatment groups. Data are mean ± SEM; p value calculated by Mann-Whitney test.

(H) Images of dissected tumors from mice treated with indicated control or treatment group.

The expression of *H2AX* in gastric cancer cell lines also positively correlated with Chk1/2 inhibitor sensitivity (Figure S4I). Gastric cancer cell lines with high *H2AX* expression were more sensitive to Chk1/2 and Wee1 inhibitors (Figures 4E, 4K, S4J, and S4K). In contrast, gastric cancer cell lines with high ploidy abnormalities were not sensitive to chemotherapeutic agents routinely used in the clinic to treat patients with gastrointestinal cancers. As an example, we show the sensitivity of gastric cancer cell lines with high and low WGD to 8 chemotherapeutic agents (Figure S4L). DDR inhibitors that did not show a significant difference among gastric cancer cell lines with high or low ploidy abnormalities are summarized in Figures S4M–S4O; there is an enrichment of ATR and ATM inhibitors among these agents.

Encouraged by these results, we validated that gastric cancer cell lines with high ploidy defects (GSU/KE39) showed greater sensitivity to Chk1/2 and Wee1 inhibitors compared to those with low ploidy defects (RPE1/AGS) (Figures 4F and 4L). These results are in agreement with the correlation plot between aneuploidy and DDR inhibitor sensitivity (Figures 4A and 4G), in which the cell lines used for validation are marked in red. Collectively, these results suggest that biomarkers of DNA DSBs/replication stress and ploidy defects could be predictive markers for DDR pathway inhibitor sensitivity in gastric cancer.

Cumulative score of ploidy abnormalities (CSPA) predicts prexasertib (Chk1/2) response

Given the predictive value of individual measures of aneuploidy and DDR pathway activity, we asked whether we could combine these parameters to better predict sensitivity to DDR inhibitors. Indeed, when we combined these parameters using a simple scoring scheme, which we refer to as the Cumulative Score of Ploidy Abnormalities (CSPA), we improved the correlation with prexasertib sensitivity (R^2 = 0.623, p = 0.0002) compared to individual values (*TP53* status, ploidy abnormalities, and *H2AX* expression) (Figures 5A and S5A). Moreover, binning the cell lines into low, medium, and high CSPA yielded a significant difference for prexasertib sensitivity, with high CSPA cell lines showing the greatest prexasertib (Chk1/2 inhibitor) sensitivity (Figures 5B and S5B). As expected, CSPA showed a strong positive correlation with DNA-PKcs (*PRKDC*), a specific marker of DDR activity (Figure S5C). The results from our cumulative score approach suggest that instead of using only one parameter, a combined score, such as CSPA, is a better predictor for DDR inhibitor sensitivity.

To understand the relationship between the DDR pathway and chemotherapy response in patients with gastric cancer, we decided to examine the previously established Recombination Proficiency Score (RPS),[28] which is derived from human gastric cancer gene expression data. RPS can predict adverse clinical features and response to chemotherapy, especially topoisomerase-I inhibiting drugs like topotecan and irinotecan, the latter of which has routinely been used in GEA. Lower RPS depicts inferior patient survival rates, higher genomic stability, and more sensitivity to chemotherapy. In line with our TCGA data analysis, mutant *TP53* gastric cancer in TCGA have lower RPS than wild-type *TP53* patients (Figure S5D), confirming that patients with mutant *TP53* gastric cancer have a poor prognosis and higher sensitivity to irinotecan. Moreover, *H2AX* expression correlates negatively with RPS score in human gastric cancer. Patients with low RPS gastric cancers display higher *H2AX* expression, reinforcing our confidence in *H2AX* expression as a biomarker for tumors exhibiting higher DNA damage and better therapy response (Figure S5E).

DDR pathway inhibitors and irinotecan combination superior to monotherapy in gastric cancer models

Chemotherapy is the backbone of most gastric cancer treatment regimens. We hypothesized that gastric cancers with high DNA DSBs/replication stress would be more sensitive to chemotherapy and DDR pathway inhibitor combinations. We therefore sought to identify chemotherapy-DDR pathway inhibitor combinations that enhance cytotoxicity, with the goal of nominating potential clinical trial concepts. KE39 cell line exhibited high DDR pathway activity, rendering it a suitable model for these experiments. Based on the recent preclinical and clinical studies, gemcitabine, a chemotherapeutic agent that generates replication stress, showed evidence of synergy when combined with DDR pathway inhibitors in small cell lung cancer, pancreatic cancer, and ovarian cancer.[29–31] Irinotecan is also a commonly used chemotherapeutic in the treatment of gastrointestinal cancers. We therefore examined the combination of either gemcitabine or irinotecan with Chk1/2 or Wee1 DDR pathway inhibitors. It is worth noting that while irinotecan is used in the clinic to treat GEA, gemcitabine is not. KE39 cells were generally more sensitive to SN38, the active metabolite of irinotecan[32] (Figure S5F), than gemcitabine-treated cells. Consistently, SN38 elicited activation of the DDR pathway as measured by H2AX, pH2AX, and pDNA-PKcs as well as replication stress as measured by pKAP1 and pRPA32 at lower doses than gemcitabine (Figure S5G, effect at 1 nM for SN38 compared to 10 nM for gemcitabine). For the DDR pathway inhibitor prexasertib, the increase in DDR/replication stress marker was first observed at 1 nM, with a more substantial increase at 5 nM (Figure S5G, right). When SN38 (2.5 nM) was combined with prexasertib or Wee1 inhibitor MK1774 (1.0 nm and 5.0 nm, respectively), the combinations showed a better effect in reducing cell viability and inducing DDR/replication stress compared with the individual monotherapies (Figures S5H and S5I). The formal interaction response analyses between prexasertib and SN38 or MK1774 and SN38 using Zero Interaction Potency (ZIP) model revealed strong additive effects with certain combination doses achieving near synergistic effect (Figure 5C). We did not observe reduced viability when combining prexasertib or MK1775 with gemcitabine (Figure S5J).

We next evaluated DDR pathway inhibitor combinations in more relevant human cancer models. Patient-derived gastric cancer organoids were treated with prexasertib or MK1775 alone or in combination with irinotecan. Combination therapy with irinotecan showed greater organoid growth inhibition than monotherapy with prexasertib or MK1775 alone (Figure 5D). We then evaluated the efficacy of these treatment

approaches *in vivo* using a gastric cancer xenograft model by injecting KE39 cells into the flanks of immunocompromised mice (Figure 5E). After xenografts grew to approximately 100 mm^3, which took about a month and a half, 6–10 mice were randomly separated into 1 vehicle control cohort and 4 treatment groups consisting of prexasertib monotherapy, MK1775 monotherapy, prexasertib + irinotecan, and MK1775 + irinotecan (Figure 5E, methods for dosing schedule). Xenograft volumes were measured weekly, and at the end of 4 weeks, all mice were sacrificed to measure tumor weights. We found that *in vivo* tumor growth was most supressed in prexasertib + irinotecan and MK1775 + irinotecan combination groups compared to monotherapy arms (Figures 5F and 5G).

Earlier in this study, we observed that p21 staining increased during premalignant to malignant progression in patients with gastric cancer and MNU-treated mice, independent of *TP53* mutation status. Interestingly, SN38 treatment in KE39 cells led to a dose-dependent induction of p21 (Figure S5K). This observation is particularly important because KE39 cells harbor a loss-of-function *TP53* mutation. Unlike the combination of SN38 with prexasertib or MK1775, the combination of gemcitabine with prexasertib or MK1775 was not able to increase DDR/replication stress markers or p21 levels (Figure S5L). These preclinical studies provide compelling evidence to pursue combination irinotecan and DDR pathway inhibitor treatment in patients with gastric cancer that exhibit high CSPA scores.

DISCUSSION

CIN constitutes the largest subtype of gastric cancer, and most of these tumors are heterogeneous, highly aneuploid, and harbor loss-of-function *TP53* mutations.[33] Different *TP53* mutations in gastric cancer are associated with various clinicopathological features and varied degree of chemoresistance.[34–36] Replication stress is commonly associated with aneuploidy, and CIN is believed to be the outcome of replication stress.[37] Moreover, aneuploidy generates replication stress-mediated DNA DSBs, activating the DDR pathway.[38] Failure of cell-cycle control can give rise to WGD.[39–41] Aneuploid cancer cells with high replication stress exhibit a high number of focal amplifications and WGD. Cells with these characteristics are intrinsically challenged with adaptive requirements but also reveal unique vulnerabilities that can be exploited for cancer therapy.[37,42] In this study, we aimed to better understand the contribution of DDR/replication stress in premalignant progression of human gastric cancer, informing early intervention and treatment strategies.

We determined that gastric premalignancy is associated with increased expression of DDR markers using matched normal, premalignant, and malignant lesions from 8 patients with gastric cancer and a carcinogen-induced (MNU) mouse model of gastric premalignancy. The cell cycle markers p53, p16, and p21 showed heterogeneity within the same tumor and between the precancerous/cancerous lesions from different samples. For both patients and mouse model, p21 gradually increased from normal to premalignant to malignant lesions independent of p53 status. p21 is downstream of canonical p53 activity, however p53-independent expression of p21 has been reported.[43] The precise mechanism of how p21 becomes activated in the absence of p53 requires further study.

Our findings reveal significantly higher expression of DDR markers *H2AX* and *TP53BP1* in gastric adenocarcinomas compared to normal tissue. H2AX is a marker of activated DNA damage and has been previously implicated in cancer progression.[10,44] The expression of *H2AX* correlates with the expression-based CIN score, and greater expression of *H2AX* is found in gastric cancer with WGD. We also showed that TP53 mutation, ploidy abnormalities, and H2AX expression correlated with DDR pathway inhibitor (Chk1/2i and Wee1i) sensitivity in gastric cancer, but when combined, these parameters yielded a better predictor for prexasertib (Chk1/2i) sensitivity. These findings suggest that ploidy abnormalities and *H2AX* expression may have clinical value as biomarkers in risk-stratifying patients with precancerous gastroesophageal lesions such as Barrett's Esophagus. Furthermore, the CSPA score may hold predictive value, identifying patients that may preferentially respond to DDR pathway inhibitors (Chk1/2i and Wee1i) sensitivity.

Using human gastric cancer cell lines, organoids, and an *in vivo* xenograft mouse model, we reinforced that combining DDR pathway inhibitors (Chk1/2i and Wee1i) with irinotecan leads to better anti-tumor responses than DDR pathway inhibitor monotherapy. Our results suggest the promising potential of combining irinotecan with the inhibitors of DDR pathways in gastric cancers that harbor increased DDR/replication stress and p21 levels. There are patient toxicities when combining cytotoxic chemotherapy with Chk1/2 or Wee1 inhibitors, mostly notably myelosuppression. To overcome this, a strategy of using low dose chemotherapy with DDR pathway inhibitors has shown promise. For example, a phase 1/II trial combining the SRA737 Chk1 inhibitor with low dose gemcitabine was well tolerated and had several radiological responses.[45] Unlike the SRA737-gemcitabine combination, a phase 1 trial of SRA737 monotherapy had no evidence of radiological responses. Overall, we hope our study will open new avenues for utilizing DDR markers and ploidy defects as a diagnostic proxy that may predict premalignant progression and sensitivity to DDR pathway inhibitors.

Limitations of the study

Our study has some limitations: (1) We only had access to human gastric specimens from 8 patients that had matched normal, premalignant, and malignant lesions for IHC studies. (2) Similarly, for IHC studies in mice, we had 4 mice treated with MNU that developed varying levels of dysplasia, limiting the power of some of our histopathological analyses. (3) We used prexasertib and MK-1775 as the Chk1/2 and Wee1 inhibitors, respectively, because these DDR inhibitors are under clinical development for solid tumors. There are newer DDR pathway inhibitors that exhibit greater target specificity and improved toxicity profiles.

STAR★METHODS

Detailed methods are provided in the online version of this paper and include the following:

- KEY RESOURCES TABLE

SUPPLEMENTAL INFORMATION

Supplemental information can be found online at https://doi.org/10.1016/j.isci.2023.108169.

ACKNOWLEDGMENTS

The authors are grateful to the pathology core facility of Brigham and Women's Hospital and Beth Israel Deaconess Medical Center for immunohistochemistry stainings. Haley Elizabeth Szewczuga at DFCI is acknowledged for editing the manuscript. Members of the N.S.S. lab are acknowledged for their support. P.S. is funded by the Finnish Cultural Foundation, Sigrid Jusélius Foundation and Instrumentarium Science Foundation. This study has been supported by the Breast Cancer Research Foundation (BCRF-21-159), Kræftens Bekæmpelse (R325-A18809 and R342-A19788), Det Frie Forskningsråd, Sundhed og Sygdom (2034-00205B) to Z.S. This study has also been supported by Augustyn Award in Digestive Cancer (American Gastroenterology Association), DeGregorio Family Foundation, Gastric Cancer Foundation, and NIDDK- National Institutes of Health (DK120930) to N.S.S. as well as philanthropy from Dave's Esophageal Fund and Nick Tierney Gastric Cancer Fund to the Sethi Lab.

AUTHOR CONTRIBUTIONS

Conceptualization: P.S. and N.S.S.; Methodology: P.S., D.P., and Z.S.; Validation: P.S., D.P., and Z.S.; Formal Analysis: P.S., D.P., P.B., Z.S., and N.S.S.; Investigation: P.S., D.P., P.B., A.L., and N.S.S.; Data Curation: P.S., Z.S., A.P., and N.S.S.; Writing – Original Draft: P.S. and N.S.S.; Writing – Review & Editing: P.S., D.P., Z.S., V.T., S.S., B.H., A.P., H.S, Z.S., J.M.C., and N.S.S.; Visualization: P.S., D.P., P.B., Z.S., and N.S.S.; Supervision: J.B.L, Z.S., J.M.C, and N.S.S.; Funding Acquisition: P.S., Z.S., and N.S.S.

DECLARATION OF INTERESTS

H.S. receives research funding from AstraZeneca, consulting fees from Dewpoint therapeutics, Merck Sharp and Dohme. J.M.C. receives research funding to his institution from Merus, Roche, Servier, and Bristol Myers Squibb. J.M.C receives research support from Merck, AstraZeneca, Esperas Pharma, Bayer, Tesaro, Arcus Biosciences, and Apexigen; he has also received honoraria for being on the advisory boards of Incyte and Blueprint Medicines and has given educational talks sponsored by Bayer, Merck, AstraZeneca, and Genentech. N.S.S. is on the scientific advisory board for and received compensation from Astrin Biosciences.

Received: February 10, 2023
Revised: August 1, 2023
Accepted: October 6, 2023
Published: October 12, 2023

REFERENCES

1. Cancer Genome Atlas Research Network (2014). Comprehensive molecular characterization of gastric adenocarcinoma. Nature *513*, 202–209. https://doi.org/10.1038/nature13480.
2. Maleki, S.S., and Röcken, C. (2017). Chromosomal Instability in Gastric Cancer Biology. Neoplasia *19*, 412–420. https://doi.org/10.1016/j.neo.2017.02.012.
3. Sohn, B.H., Hwang, J.E., Jang, H.J., Lee, H.S., Oh, S.C., Shim, J.J., Lee, K.W., Kim, E.H., Yim, S.Y., Lee, S.H., et al. (2017). Clinical Significance of Four Molecular Subtypes of Gastric Cancer Identified by The Cancer Genome Atlas Project. Clin. Cancer Res. *23*, 4441–4449. https://doi.org/10.1158/1078-0432.CCR-16-2211.
4. Domínguez-Kelly, R., Martín, Y., Koundrioukoff, S., Tanenbaum, M.E., Smits, V.A.J., Medema, R.H., Debatisse, M., and Freire, R. (2011). Wee1 controls genomic stability during replication by regulating the Mus81-Eme1 endonuclease. J. Cell Biol. *194*, 567–579. https://doi.org/10.1083/jcb.201101047.
5. Elvers, I., Hagenkort, A., Johansson, F., Djureinovic, T., Lagerqvist, A., Schultz, N., Stoimenov, I., Erixon, K., and Helleday, T. (2012). CHK1 activity is required for continuous replication fork elongation but not stabilization of post-replicative gaps after UV irradiation. Nucleic Acids Res. *40*, 8440–8448. https://doi.org/10.1093/nar/gks646.
6. Banerji, U., Plummer, E.R., Moreno, V., Ang, J.E., Quinton, A., Drew, Y., Hernández, T., Roda, D., Carter, L., Navarro, A., et al. (2019). A phase I/II first-in-human trial of oral SRA737 (a Chk1 inhibitor) given in combination with low-dose gemcitabine in subjects with advanced cancer. J. Clin. Oncol. *37*, 3095. https://doi.org/10.1200/JCO.2019.37.15_suppl.3095.
7. Macheret, M., and Halazonetis, T.D. (2015). DNA replication stress as a hallmark of cancer. Annu. Rev. Pathol. *10*, 425–448. https://doi.org/10.1146/annurev-pathol-012414-040424.
8. Gupta, A., Hunt, C.R., Chakraborty, S., Pandita, R.K., Yordy, J., Ramnarain, D.B., Horikoshi, N., and Pandita, T.K. (2014). Role of 53BP1 in the regulation of DNA double-strand break repair pathway choice. Radiat. Res. *181*, 1–8. https://doi.org/10.1667/RR13572.1.
9. Mah, L.J., El-Osta, A., and Karagiannis, T.C. (2010). gammaH2AX: a sensitive molecular marker of DNA damage and repair. Leukemia *24*, 679–686. https://doi.org/10.1038/leu.2010.6.
10. Bartkova, J., Horejsí, Z., Koed, K., Krämer, A., Tort, F., Zieger, K., Guldberg, P., Sehested, M., Nesland, J.M., Lukas, C., et al. (2005). DNA damage response as a candidate anti-cancer barrier in early human tumorigenesis. Nature *434*, 864–870. https://doi.org/10.1038/nature03482.
11. Sethi, N.S., Kikuchi, O., Duronio, G.N., Stachler, M.D., McFarland, J.M., Ferrer-Luna, R., Zhang, Y., Bao, C., Bronson, R., Patil, D., et al. (2020). Early TP53 alterations engage environmental exposures to promote gastric premalignancy in an integrative mouse model. Nat. Genet. *52*, 219–230. https://doi.org/10.1038/s41588-019-0574-9.
12. Stachler, M.D., and Bass, A.J. (2020). Can Genomic Sequencing Identify High-Risk Barrett's Esophagus Earlier Than Pathologists? Cancer Cell *38*, 626–628. https://doi.org/10.1016/j.ccell.2020.10.020.
13. Stachler, M.D., Camarda, N.D., Deitrick, C., Kim, A., Agoston, A.T., Odze, R.D., Hornick, J.L., Nag, A., Thorner, A.R., Ducar, M., et al. (2018). Detection of Mutations in Barrett's Esophagus Before Progression to High-Grade Dysplasia or Adenocarcinoma. Gastroenterology *155*, 156–167. https://doi.org/10.1053/j.gastro.2018.03.047.
14. Stachler, M.D., Taylor-Weiner, A., Peng, S., McKenna, A., Agoston, A.T., Odze, R.D., Davison, J.M., Nason, K.S., Loda, M., Leshchiner, I., et al. (2015). Paired exome analysis of Barrett's esophagus and adenocarcinoma. Nat. Genet. *47*, 1047–1055. https://doi.org/10.1038/ng.3343.
15. Weaver, J.M.J., Ross-Innes, C.S., Shannon, N., Lynch, A.G., Forshew, T., Barbera, M., Murtaza, M., Ong, C.A.J., Lao-Sirieix, P., Dunning, M.J., et al. (2014). Ordering of mutations in preinvasive disease stages of esophageal carcinogenesis. Nat. Genet. *46*, 837–843. https://doi.org/10.1038/ng.3013.
16. Sahgal, P., Huffman, B.M., Patil, D.T., Chatila, W.K., Yaeger, R., Cleary, J.M., and Sethi, N.S. (2021). Early TP53 Alterations Shape Gastric and Esophageal Cancer Development. Cancers *13*, 5915. https://doi.org/10.3390/cancers13235915.
17. Liu, Y., Sethi, N.S., Hinoue, T., Schneider, B.G., Cherniack, A.D., Sanchez-Vega, F., Seoane, J.A., Farshidfar, F., Bowlby, R., Islam, M., et al. (2018). Comparative Molecular Analysis of Gastrointestinal Adenocarcinomas. Cancer Cell *33*, 721–735.e8. https://doi.org/10.1016/j.ccell.2018.03.010.
18. Chen, J. (2016). The Cell-Cycle Arrest and Apoptotic Functions of p53 in Tumor Initiation and Progression. Cold Spring Harb. Perspect. Med. *6*, a026104. https://doi.org/10.1101/cshperspect.a026104.
19. TCGA. https://www.cancer.gov/about-nci/organization/ccg/research/structural-genomics/tcga.
20. Lauren, P. (1965). The Two Histological Main Types of Gastric Carcinoma: Diffuse and So-Called Intestinal-Type Carcinoma. An Attempt at a Histo-Clinical Classification. Acta Pathol. Microbiol. Scand. *64*, 31–49. https://doi.org/10.1111/apm.1965.64.1.31.
21. Carter, S.L., Eklund, A.C., Kohane, I.S., Harris, L.N., and Szallasi, Z. (2006). A signature of chromosomal instability inferred from gene expression profiles predicts clinical outcome in multiple human cancers. Nat. Genet. *38*, 1043–1048. https://doi.org/10.1038/ng1861.
22. Barretina, J., Caponigro, G., Stransky, N., Venkatesan, K., Margolin, A.A., Kim, S., Wilson, C.J., Lehár, J., Kryukov, G.V., Sonkin, D., et al. (2012). The Cancer Cell Line Encyclopedia enables predictive modelling of anticancer drug sensitivity. Nature *483*, 603–607. https://doi.org/10.1038/nature11003.
23. Cohen-Sharir, Y., McFarland, J.M., Abdusamad, M., Marquis, C., Bernhard, S.V., Kazachkova, M., Tang, H., Ippolito, M.R., Laue, K., Zerbib, J., et al. (2021). Aneuploidy renders cancer cells vulnerable to mitotic checkpoint inhibition. Nature *590*, 486–491. https://doi.org/10.1038/s41586-020-03114-6.
24. Ghandi, M., Huang, F.W., Jané-Valbuena, J., Kryukov, G.V., Lo, C.C., McDonald, E.R., 3rd, Barretina, J., Gelfand, E.T., Bielski, C.M., Li, H., et al. (2019). Next-generation characterization of the Cancer Cell Line Encyclopedia. Nature *569*, 503–508. https://doi.org/10.1038/s41586-019-1186-3.
25. White, D.E., Negorev, D., Peng, H., Ivanov, A.V., Maul, G.G., and Rauscher, F.J., 3rd (2006). KAP1, a novel substrate for PIKK family members, colocalizes with numerous damage response factors at DNA lesions. Cancer Res. *66*, 11594–11599. https://doi.org/10.1158/0008-5472.CAN-06-4138.
26. Angius, G., Tomao, S., Stati, V., Vici, P., Bianco, V., and Tomao, F. (2020). Prexasertib, a checkpoint kinase inhibitor: from preclinical data to clinical development. Cancer Chemother. Pharmacol. *85*, 9–20. https://doi.org/10.1007/s00280-019-03950-y.
27. Corsello, S.M., Nagari, R.T., Spangler, R.D., Rossen, J., Kocak, M., Bryan, J.G., Humeidi, R., Peck, D., Wu, X., Tang, A.A., et al. (2020). Discovering the anti-cancer potential of non-oncology drugs by systematic viability profiling. Nat. Cancer *1*, 235–248. https://doi.org/10.1038/s43018-019-0018-6.
28. Pitroda, S.P., Pashtan, I.M., Logan, H.L., Budke, B., Darga, T.E., Weichselbaum, R.R., and Connell, P.P. (2014). DNA repair pathway gene expression score correlates with repair proficiency and tumor sensitivity to chemotherapy. Sci. Transl. Med. *6*, 229ra42. https://doi.org/10.1126/scitranslmed.3008291.
29. Sen, T., Della Corte, C.M., Milutinovic, S., Cardnell, R.J., Diao, L., Ramkumar, K., Gay, C.M., Stewart, C.A., Fan, Y., Shen, L., et al. (2019). Combination Treatment of the Oral CHK1 Inhibitor, SRA737, and Low-Dose Gemcitabine Enhances the Effect of Programmed Death Ligand 1 Blockade by Modulating the Immune Microenvironment in SCLC. J. Thorac. Oncol. *14*, 2152–2163. https://doi.org/10.1016/j.jtho.2019.08.009.
30. Wallez, Y., Dunlop, C.R., Johnson, T.I., Koh, S.B., Fornari, C., Yates, J.W.T., Bernaldo de Quirós Fernández, S., Lau, A., Richards, F.M., and Jodrell, D.I. (2018). The ATR Inhibitor AZD6738 Synergizes with Gemcitabine In Vitro and In Vivo to Induce Pancreatic Ductal Adenocarcinoma Regression. Mol. Cancer Ther. *17*, 1670–1682. https://doi.org/10.1158/1535-7163.MCT-18-0010.
31. Konstantinopoulos, P.A., Cheng, S.C., Wahner Hendrickson, A.E., Penson, R.T., Schumer, S.T., Doyle, L.A., Lee, E.K., Kohn, E.C., Duska, L.R., Crispens, M.A., et al. (2020). Berzosertib plus gemcitabine versus gemcitabine alone in platinum-resistant high-grade serous ovarian cancer: a multicentre, open-label, randomised, phase 2 trial. Lancet Oncol. *21*, 957–968. https://doi.org/10.1016/S1470-2045(20)30180-7.
32. Ramesh, M., Ahlawat, P., and Srinivas, N.R. (2010). Irinotecan and its active metabolite, SN-38: review of bioanalytical methods and recent update from clinical pharmacology perspectives. Biomed. Chromatogr. *24*, 104–123. https://doi.org/10.1002/bmc.1345.
33. Giam, M., and Rancati, G. (2015). Aneuploidy and chromosomal instability in cancer: a jackpot to chaos. Cell Div. *10*, 3. https://doi.org/10.1186/s13008-015-0009-7.
34. Xu, H.Y., Xu, W.L., Wang, L.Q., Chen, M.B., and Shen, H.L. (2014). Relationship between p53 status and response to chemotherapy in patients with gastric cancer: a meta-analysis. PLoS One *9*, e95371. https://doi.org/10.1371/journal.pone.0095371.

35. Tahara, T., Shibata, T., Okamoto, Y., Yamazaki, J., Kawamura, T., Horiguchi, N., Okubo, M., Nakano, N., Ishizuka, T., Nagasaka, M., et al. (2016). Mutation spectrum of TP53 gene predicts clinicopathological features and survival of gastric cancer. Oncotarget *7*, 42252–42260. https://doi.org/10.18632/oncotarget.9770.

36. Shi, W.J., and Gao, J.B. (2016). Molecular mechanisms of chemoresistance in gastric cancer. World J. Gastrointest. Oncol. *8*, 673–681. https://doi.org/10.4251/wjgo.v8.i9.673.

37. Zhu, J., Tsai, H.J., Gordon, M.R., and Li, R. (2018). Cellular Stress Associated with Aneuploidy. Dev. Cell *44*, 420–431. https://doi.org/10.1016/j.devcel.2018.02.002.

38. Ohashi, A., Ohori, M., Iwai, K., Nakayama, Y., Nambu, T., Morishita, D., Kawamoto, T., Miyamoto, M., Hirayama, T., Okaniwa, M., et al. (2015). Aneuploidy generates proteotoxic stress and DNA damage concurrently with p53-mediated post-mitotic apoptosis in SAC-impaired cells. Nat. Commun. *6*, 7668. https://doi.org/10.1038/ncomms8668.

39. Quinton, R.J., DiDomizio, A., Vittoria, M.A., Kotýnková, K., Ticas, C.J., Patel, S., Koga, Y., Vakhshoorzadeh, J., Hermance, N., Kuroda, T.S., et al. (2021). Publisher Correction: Whole-genome doubling confers unique genetic vulnerabilities on tumour cells. Nature *593*, E15. https://doi.org/10.1038/s41586-021-03591-3.

40. Goyal, A., Takaine, M., Simanis, V., and Nakano, K. (2011). Dividing the spoils of growth and the cell cycle: The fission yeast as a model for the study of cytokinesis. Cytoskeleton (Hoboken) *68*, 69–88. https://doi.org/10.1002/cm.20500.

41. Dewhurst, S.M., McGranahan, N., Burrell, R.A., Rowan, A.J., Grönroos, E., Endesfelder, D., Joshi, T., Mouradov, D., Gibbs, P., Ward, R.L., et al. (2014). Tolerance of whole-genome doubling propagates chromosomal instability and accelerates cancer genome evolution. Cancer Discov. *4*, 175–185. https://doi.org/10.1158/2159-8290.CD-13-0285.

42. Quinton, R.J., DiDomizio, A., Vittoria, M.A., Kotýnková, K., Ticas, C.J., Patel, S., Koga, Y., Vakhshoorzadeh, J., Hermance, N., Kuroda, T.S., et al. (2021). Whole-genome doubling confers unique genetic vulnerabilities on tumour cells. Nature *590*, 492–497. https://doi.org/10.1038/s41586-020-03133-3.

43. Origanti, S., Cai, S.R., Munir, A.Z., White, L.S., and Piwnica-Worms, H. (2013). Synthetic lethality of Chk1 inhibition combined with p53 and/or p21 loss during a DNA damage response in normal and tumor cells. Oncogene *32*, 577–588. https://doi.org/10.1038/onc.2012.84.

44. Krishnan, V., Lim, D.X.E., Hoang, P.M., Srivastava, S., Matsuo, J., Huang, K.K., Zhu, F., Ho, K.Y., So, J.B.Y., Khor, C., et al. (2020). DNA damage signalling as an anti-cancer barrier in gastric intestinal metaplasia. Gut *69*, 1738–1749. https://doi.org/10.1136/gutjnl-2019-319002.

45. Jones, R., Plummer, R., Moreno, V., Carter, L., Roda, D., Garralda, E., Kristeleit, R., Sarker, D., Arkenau, T., Roxburgh, P., et al. (2023). A Phase I/II Trial of Oral SRA737 (a Chk1 Inhibitor) Given in Combination with Low-Dose Gemcitabine in Patients with Advanced Cancer. Clin. Cancer Res. *29*, 331–340. https://doi.org/10.1158/1078-0432.CCR-22-2074.

46. Yadav, B., Wennerberg, K., Aittokallio, T., and Tang, J. (2015). Searching for Drug Synergy in Complex Dose-Response Landscapes Using an Interaction Potency Model. Comput. Struct. Biotechnol. J. *13*, 504–513. https://doi.org/10.1016/j.csbj.2015.09.001.

47. Ianevski, A., Giri, A.K., and Aittokallio, T. (2022). SynergyFinder 3.0: an interactive analysis and consensus interpretation of multi-drug synergies across multiple samples. Nucleic Acids Res. *50*, W739–W743. https://doi.org/10.1093/nar/gkac382.

48. Colaprico, A., Silva, T.C., Olsen, C., Garofano, L., Cava, C., Garolini, D., Sabedot, T.S., Malta, T.M., Pagnotta, S.M., Castiglioni, I., et al. (2016). TCGAbiolinks: an R/Bioconductor package for integrative analysis of TCGA data. Nucleic Acids Res. *44*, e71. https://doi.org/10.1093/nar/gkv1507.

STAR★METHODS

KEY RESOURCES TABLE

REAGENT or RESOURCE	SOURCE	IDENTIFIER
Antibodies		
Rabbit anti-Ki67	Biocare Medical	Cat# CRM325-5b6; RRID:AB_2721189
Rabbit anti-H2AX	Cell Signaling Technology	Cat# 7631; RRID: AB_10860771
Rabbit anti-pH2AX ser139	Cell Signaling Technology	Cat# 9718; RRID:AB_2118009
Mouse anti-pH2AX ser139	Cell Signaling Technology	Cat# 80312; RRID:AB_2799949
Mouse anti-53BP1	Millipore	Cat# 3802; RRID:AB_2206767
Mouse anti-p53	Cell Signaling Technology	Cat# 48818; RRID:AB_2713958
Rabbit anti-p53	Abcam	Cat# ab1431; RRID:AB_301090
Mouse anti-p16INK4	Abcam	Cat# ab54210; RRID:AB_881819
Rabbit anti-p21	Cell Signaling Technology	Cat# 2947; RRID:AB_823586
Rabbit anti-p21	Abcam	Cat# ab188224; RRID:AB_2734729
Rabbit anti-pTIF1β/pKAP1 (Ser824)	Cell Signaling Technology	Cat# 4127S; RRID:AB_2209906
Rabbit anti-TIF1β/KAP1	Cell Signaling Technology	Cat# 4124S; RRID:AB_2209886
anti-Rabbit IgG Alexa Fluor 488	Life tech	Cat# A11008; RRID:AB_143165
anti-Mouse IgG Alexa Fluor 568	Life tech	Cat# A11004; RRID:AB_2534072
Rabbit anti-pDNA-PKcs	Cell Signaling Technology	Cat# 12311S; RRID:AB_2797881
Rabbit anti-αTubulin	Cell Signaling Technology	Cat# 2125; RRID:AB_2619646
Rabbit anti-RPA32	Bethyl	Cat# A300-244A; RRID:AB_185548
Rabbit anti-pRPA32 (S33)	Bethyl	Cat# A300-246A; RRID:AB_2180847
Donkey anti-mouse IRDye 800CW	LI-COR	Cat# 926-32212; RRID:AB_621847
Donkey anti-mouse IRDye 680RD	LI-COR	Cat# 926-68072; RRID:AB_10953628
Donkey anti-rabbit IRDye 800CW	LI-COR	Cat# 926-32213; RRID:AB_621848
Donkey anti-rabbit IRDye 680RD	LI-COR	Cat# 926-68073; RRID:AB_10954442
Biological samples		
Human gastric cancer samples	Dana-Farber Cancer Institute	N/A
Carcinogen-induced (MNU) mouse model	Dana-Farber Cancer Institute	N/A
Human gastric cancer organoids	This paper	N/A
Nude mice subcutaneous tumors	This paper	N/A
Chemicals, peptides, and recombinant proteins		
prexasertib	Selleck	Cat# S7178
AZD6738	Selleck	Cat# S7693
MK1775	Selleck	Cat# S1525
gemcitabine	Selleck	Cat# S1149
SN-38	Selleck	Cat# S4908
irinotecan	Hikma Pharmaceuticals	Cat# 00143958301
Matrigel	Corning	Cat# 356231
Paraformaldehyde	ThermoScientific	Cat# 28908
DMSO	MilliporeSigma	Cat# D2650
Crystal violet	Sigma Aldrich	Cat# HT901
Critical commercial assays		
CellTiter-Glo	Promega	Cat# G7572

(*Continued on next page*)

Continued

REAGENT or RESOURCE	SOURCE	IDENTIFIER
BCA Protein Assay Kit	Thermo Scientific	Cat# 23227
Experimental models: Cell lines		
HGC27	Broad Institute	RRID:CVCL_1279
AGS	Broad Institute	RRID:CVCL_0139
GSU	Broad Institute	RRID:CVCL_8877
KE39	Broad Institute	RRID:CVCL_3385
NUGC3	Broad Institute	RRID:CVCL_1612
RPE1	ATCC	RRID:CVCL_4388
Experimental models: Organisms/strains		
NU/J (Homo) -/- Homozygous mice	Jackson Laboratory	Cat# 002019
Software and algorithms		
GraphPad Prism 9	GraphPad	https://www.graphpad.com/
ImageJ	NIH	https://ImageJ.nih.gov/ij/
SynergyFinder 3.0	FIMM	https://synergyfinder.fimm.fi/
TCGABiolinks R package	Bioconductor	https://bioconductor.org/packages/release/bioc/html/TCGAbiolinks.html
TCGA	NCI	https://www.cancer.gov/ccg/research/genome-sequencing/tcga
cBioPortal	Memorial Sloan Kettering Cancer Center (MSK)	https://www.cbioportal.org/
DepMap	Broad Institute	https://depmap.org/portal/

RESOURCE AVAILABILITY

Lead contact

Further information and requests for resources and reagents should be directed to and will be fulfilled by the lead contact, Nilay S. Sethi (nilay_sethi@dfci.harvard.edu).

Materials availability

Human gastric cancer organoids generated in this study may be available after signing an MTA.

Data and code availability

- All data reported in this paper will be shared by the lead contact upon request.
- This paper does not report original code.
- Any additional information required to reanalyze the data reported in this paper is available from the lead contact upon request.

EXPERIMENTAL MODEL AND STUDY PARTICIPANT DETAILS

Human normal, premalignant and malignant gastric lesion collection

All human samples were obtained through IRB protocol 001467. Criteria for patient selection included the presence of normal, premalignant, and malignant gastric tissue on the same specimen, which yielded 8 patients. These samples then underwent histopathological evaluation, including IHC, as described in the STAR Methods and the results were reviewed/scored by GI pathologist D.T.P.

Carcinogen-induced (MNU) mouse model of gastric premalignancy and cancer

Mouse specimens were obtained from the stomachs of mice that were part of experiments conducted in our prior study{Sethi, 2020 #208}. Briefly, all treated mice were subjected to drinking water containing 240ppm of N-methyl-N-nitrosourea (MNU; biokemix) scheduled every other week for 6 weeks continuously for 1 year. Mice were euthanized at the endpoint of the experiment, and stomachs were harvested for histopathological and immunohistochemical analyses as well as organoid generation.

In-vivo mouse xenograft model

All animal experiments were conducted in accordance with the Institutional Animal Care and use committee approved animal protocols (#11-009) at the Dana Farber Cancer Institute (Boston, MA) in compliance with NIH guidelines. Nude mice (Male, 4 weeks old, Stock: 002019) were obtained from Jackson Laboratory and acclimatized for 2 weeks in DFCI Animal research facility before xenograft injections. KE39 cells were detected as pathogen free and cultured in RPMI1640 supplemented with 10% FBS. Cells were washed with serum free medium and resuspended in serum free medium mixed with an equal amount of Matrigel (356231 Corning). Mice were injected with 5 million KE39 cells per injection, with two distinct injections in the flank of each mouse. Tumors were monitored twice weekly using electronic calipers, and tumor volumes were calculated using the formula: volume = 0.5 × length × width2. When the tumor volume reached approximately 100mm, mice were randomized into treatment and control groups (n = 6) and treated with the indicated drugs. Prexasertib was given subcutaneously (10 mg/kg) twice daily on a 3 days on/4 days off schedule, for 3 cycles. MK-1775 was given orally (30 mg/kg) once daily for 3 weeks. Irinotecan was administered intra-peritoneally (40 mg/kg) every 4 days for 3 weeks. Tumor volumes were measured twice weekly.

Human gastric cancer organoids

Human gastric cancer samples were obtained from the Department of Surgery, under approval (protocol 13-189) by the Internal Review Board of the Dana-Farber Cancer Institute, Boston, MA, USA, and used to make neoplastic human gastric organoids. The gastric tissue after surgery was rinsed with ice-cold phosphate-buffered saline (PBS) in a 90-mm petri dish, washed with ~20 ml of ice-cold PBS in a 50-ml tube by vigorous shaking, and then rinsed again with ice-cold PBS in a 90-mm petri dish. After washing, tissue was transferred to a 35-mm petri dish in a biological tissue culture hood and then minced with fine scissors. One milliliter of collagenase (Invitrogen) solution was added to suspend tissue fragments, and the petri dish was incubated in a cell culture incubator (37°C) with vigorous mixing every 5 to 10 min using a 1000-μl pipette. The epithelial units were passed through a 70-μm cell strainer (BD) using a 1000-μl pipette, and the strainer was washed with 9 ml of washing media [penicillin (100 U/ml), streptomycin (0.1 mg/ml), L-glutamine (2 mM), and FBS (10% in DMEM/F-12; Invitrogen) with Hepes]. This filtrate was transferred to a 1.5-ml centrifuge tube, centrifuged at 200g for 5 min, and placed on ice, and the epithelial units were resuspended in Matrigel (15 μl per well; Corning). Fifteen microliters of cell Matrigel suspension was then placed in the center of each well of a 24-well plate using a 20-μl pipette and spread with a pipette tip. To polymerize the Matrigel, plates were incubated upside down to avoid attachment of epithelial units to the plate surface. After 3 to 5 min, plates were returned to the upright orientation, and 500 μl of 50% human L-WRN conditioned medium were added to each well, and the medium was subsequently changed at least every 48 hours. Human L_WRN medium is a 1:1 mix of L WRN conditioned medium and advanced DMEM/F-12 with 20% FBS supplemented with antibiotics Primocin (100 μg/ml; InvivoGen), Normocin (100 μg/ml; InvivoGen); serum-free supplements 1X B27 [Thermo Fisher Scientific (Gibco)] and 1X N2 [Thermo Fisher Scientific (Gibco)]; and chemical supplements 10 mM nicotinamide (Sigma-Aldrich), 500 mM N-acetylcysteine (Sigma-Aldrich), hormone 50 mM [Leu15]-Gastrin (Sigma-Aldrich), growth factor FGF10 (recombinant human) (100 μg/ml; Thermo Fisher Scientific), and 500 nM A-83-01 (Sigma-Aldrich), which is an inhibitor of the transforming growth factor–β receptors ALK4, 5, and 7, and 10 mM rho-associated coiled-coil protein kinase (ROCK) inhibitor Y-27632 (Sigma-Aldrich). For passage, gastric cancer organoids were dispersed by trypsin-EDTA and transferred to fresh Matrigel. Passage was performed every 3 to 4 days with a 1:3 to 1:5 split ratio. After treating the organoids for three days with indicated drugs concentrations as monotherapy or combination therapy, cell viability was measured using the CellTiter-Glo assay.

Cell lines and cell culture

Human gastric cancer cell lines were obtained from the CCLE core facility (BROAD Institute, Cambridge), which obtained them directly from commercial sources and authenticated the lines using standard short tandem repeat analysis. RPE1 cells were obtained from the American Type Culture Collection (ATCC). RPE1 cells were grown in DMEM-F12 (Life Technologies, #10565042) supplemented with 10% FBS and 1% penicillin/streptomycin. HGC27 cells were grown in DMEM (Life Technologies, #11965118) supplemented with 10% FBS and 1% penicillin/streptomycin. AGS, GSU, KE39, and NUGC3 were grown in RPMI 1640 (Life Technologies, #11875119) supplemented with 10% FBS and 1% penicillin/streptomycin. Cells lines were maintained in a humidified 37°C incubator with 5% CO2 and routinely tested for mycoplasma contamination (Lonza #LT07-118).

METHOD DETAILS

Histopathology and immunohistochemistry

For immunostaining, antigen retrieval was performed using a sodium citrate buffer (pH6), Trilogy (Sigma Aldrich Cell Marque), or Tris-EDTA, pH 9.0. Slides were permeabilized using a 0.2% Triton X100 for 30 minutes at room temperature and blocked with donkey serum for 1 hour. The primary antibodies used for immunohistochemistry were: Human tissue- rabbit anti-ki67 (1:1000, Biocare Medical, #CRM325-5b6), rabbit anti-H2AX (1:1000, CST, #7631), rabbit anti-pH2AX ser139 (1:1000, CST, #9718), mouse anti-53BP1 (1:1000, Millipore, #3802), mouse anti-p53 (1:1000, CST, #48818), mouse anti-p16INK4 (1:1000, Abcam, #ab54210), rabbit anti-p21 (1:1000, CST, #2947), Murine tissue- rabbit anti-ki67 (1:1000, Biocare Medical, #CRM325-5b6), rabbit anti-pH2AX ser139, (1:1000, CST, #9718), rabbit anti-p53 (1:1000, Abcam, #ab1431), rabbit anti-p21 (1:1000, Abcam, #ab188224). Binding of primary antibody was detected with 3,39-diamino-benzidine-tetrahydrochloride-dihydrate and counterstained with hematoxylin. Images were acquired with Leica DM750 microscope. The slides were reviewed by expert GI pathologist (D.T.P.). For each antibody, the percentage positive cells (<=5%, 6-50%, and >50%) were assessed along with intensity of staining (weak,

moderate, or strong). For p53, overexpression and null pattern of expression were considered "abnormal" expression while weak, patchy staining was considered normal/wild-type expression. Cytoplasmic and nuclear p16 expression were assessed in all cases.

Immunofluorescence

Cells were plated on glass-Teflon microscope slide (Tekdon, #518plain) and the next day treated with either DMSO or different concentrations of prexasertib (Selleck, #S7178) for 24 hours. Cells were then washed and fixed with 4% paraformaldehyde (PFA) for 15 minutes at room temperature, blocked and permeabilized PBS-BSA + 0.3% Triton X-100 for 15 minutes at room temperature, and incubated with primary antibodies (rabbit anti-pTIF1β/pKAP1 (Ser824) (1:500, CST # 4127S) and Mouse anti-pH2AX (1:600, CST #80312) in PBS-BSA overnight at +4°C. After 3 washes with PBS, secondary antibodies; anti-Rabbit IgG Alexa Fluor 488 (Life tech #A11008) and anti-Mouse IgG Alexa Fluor 568 (Life tech #A11004), diluted 1:300 in PBS-BSA with DAPI (1:1000) for 2 hours at room temperature. Finally, the cells were washed with PBS 3 times, mounted, and covered in aluminum foil for imaging.

Microscopy and image quantification

Immunofluorescence imaging was performed using Nikon Eclipse Ti2 Series inverted microscope (×40 objective). NIS-Elements AR software was used to acquire the images. DAPI channel was used to focus the cells, and the images for 488 (pKAP1) and 567 (pH2AX) channels were acquired, keeping the same exposure across the samples. For image analysis, the 16-bit images were converted to 2-bit images in ImageJ, followed by 'hole filling' and segmentation (watershed) commands. The cells were then automatically recognized and counted using 'analyze particles', and the file was saved as an 'image mask'. Finally, the image mask was overlaid on the original green (488) and red (567) split channels, and the 'measure' command was used to get the mean fluorescence intensity from each cell.

Cell proliferation assay and inhibitors

For IC50 experiments, 1000 cells were plated in a flat-bottom 96-well plate. Cells were treated with either vehicle (DMSO) or different concentrations of the inhibitors. Luminescence was measured using CellTiter-Glo (Promega, #G7572) for ATP amount after 3 days, and final readings were normalized with Day 1 luminescence readings. For colony formation assay, $2x10^4$-1x10^5 cells were plated in 6-well plates. Cells were then treated with DMSO or inhibitors. After 4-6 days, cells were fixed in 1% paraformaldehyde for 15 minutes at room temperature, washed twice with PBS, and stained with 0.1% crystal violet solution in ethanol (Sigma Aldrich, #HT901) for 15 minutes at room temperature. ImageJ was used to quantify the mean intensity of the scanned plates. The following drug agents were used in the study: prexasertib (Selleck, #S7178), AZD6738 (Selleck, #S7693), MK1775 (Selleck, #S1525), gemcitabine (Selleck, #S1149), and SN-38 (Selleck, #S4908). The synergy analysis was performed using the zero interaction potency (ZIP) model.[46] Briefly, different concentrations of each drug were used, either alone or in combination. After three days of treatment, cell viability was measured using the CellTiter-Glo assay. The results were analyzed using SynergyFinder 3.0.[47]

Immunoblot

Cells were washed with cold phosphate buffer saline (PBS) and lysed in RIPA buffer (Sigma- Aldrich, #R0278-50ML) supplemented with a protease inhibitor (Roche, #11873580001) and phosphatase inhibitor (CST #5870S). Protein extracts were separated using SDS-PAGE under denaturing conditions (8–16% Novex™ Wedgewell™ Tris-Glycine Gels) and were transferred to PVDF membranes (iBlot2™ PVDF Regular Stacks). Membranes were blocked with blocking buffer (InterceptTM Blocking buffer, #927-60001) and incubated with the primary antibodies diluted in blocking buffer and incubated overnight at +4°C. After primary antibody incubation: rabbit anti-pTIF1β/pKAP1 (Ser824) (1:1000, CST # 4127S), rabbit anti-TIF1β/KAP1 (1:1000, CST # 4124S), rabbit anti-H2AX (1:1000, CST #7631), mouse anti-pH2AX (1:1000, CST #80312), rabbit anti-pDNA-PKcs (1:1000, CST, #12311S), rabbit anti-αTubulin (1:5000, CST, #2125), rabbit anti-p21 (1:500, CST, #2947S), rabbit anti-RPA32 (1:1000, Bethyl, A300-244A) and rabbit anti-pRPA32 (1:1000, Bethyl, A300-246A) membranes were washed 3 times with TBST and incubated with fluorophore-conjugated secondary antibodies diluted (1:10,000) in blocking buffer at room temperature for 1 hour. Membranes were then scanned using an infrared imaging system (Odyssey; LI-COR Biosciences). The following secondary antibodies were used: donkey anti-mouse IRDye 800CW (LI-COR, 926-32212), donkey anti-mouse IRDye 680RD (LI-COR, 926-68072), donkey anti-rabbit IRDye 800CW (LI-COR, 926-32213), and donkey anti-rabbit IRDye 680RD (LI-COR, 926-68073).

TCGA analysis

For the TCGA dataset FPKM-UQ, normalized expression values were downloaded from the TCGA data portal and subtype information was accessed using TCGABiolinks R package.[48] The following subtypes were defined: CIN (chromosomal instability), GS (genomically stable), EBV (Epstein–Barr virus-positive), MSI (microsatellite instability), and HM-SNV (hypermutated-single-nucleotide variant predominant), based on.[17] World Health Organization (WHO) histological classification was available for these samples and Lauren-classification was determined based on WHO classification. *TP53* mutation status was downloaded from cBioPortal and only pathogenic mutations were treated as mutant cases.

Drug sensitivity and correlation analysis

The gene expression, aneuploidy, and drug sensitivity data were downloaded (22Q2 data release from DepMap website of Broad Institute [https://depmap.org]). For the drug sensitivity analysis, the cell lines were divided into a high or low group based on quartiles of the

expression of gene of interest, score, or feature. The difference between the mean of sensitivity for the two groups was plotted, and the p-value was calculated using the unpaired t-test. For the correlation analysis, the continuous data were plotted, and R-squared/p-value was calculated using simple linear correlation analysis.

QUANTIFICATION AND STATISTICAL ANALYSIS

ImageJ was used to quantify the immunofluorescence images. All the statistical analyses were performed using GraphPad Prism, version 9.0 (GraphPad Software). To compare the difference between two groups, independent sample t test, paired t-test, Mann–Whitney U test or ANOVA test was used. $p<0.05$ was considered statistically significant.